AC

SNUTP 93-91

SNUTP 93-91
SCU 9406

Crossing Constraint in Kaon Production and Capture

Chueng-Ryong Ji *
Dept. of Physics, Seoul National University
Seoul 151-742, Korea

Robert A. Williams
Dept. of Physics, Hampton University
Hampton, Virginia 23668, USA
and
Continuous Electron Beam Accelerator Facility
1200 Jefferson Avenue, Newport News, Va. 23606, USA

Stephen R. Cotanch
Dept. of Physics, North Carolina State University
Raleigh, North Carolina 27695-8202, USA

Abstract

The crossing property of the S-matrix is discussed and employed as a constraint in the analyses of kaon photo/electro production and capture processes.

*Permanent address is the Department of Physics, North Carolina State University, Raleigh, NC 27695-8202.

I Introduction

A fundamental relation between nuclear, particle physics and astrophysics has developed with the recognition that nuclear and particle physics are essential in understanding the history of the universe and its contents [1]. Accordingly, both nuclear and high energy particle laboratory experiments are pivotal to understand various reaction mechanisms in the early universe. For example, if the Superconducting Super Collider (SSC) project near Dallas, Texas would be completed, proton beam energies of the order of 10 TeV would be achieved. This energy corresponds to a temperature of 10^{17}K, which is the temperature of the early universe at 10^{-15}s after the big bang. Thus, the particle reaction mechanisms occuring in the early universe can be studied at the SSC. Likewise, the Continuous Electron Beam Accelerator Facility (CEBAF) which is being built in Newport News, Virginia can study the early universe at 10^{-5}s after the big bang, corresponding to a temperature of 10^{12}K. Since the quarks and gluons are hadronized at this temperature, CEBAF will be an important laboratory to test theoretical models of hadron structure and reactions manifest in the early universe. Therefore, the experimental data from CEBAF will be quite invaluable both for theoretical model studies of hadron reactions and studies of the early universe at 10^{-5}s after the big bang.

While Quantum Chromodynamics (QCD) is accepted as the correct theory of strong interactions, it is still fruitful to investigate hadronic models based on Quantum Hadrodynamics (QHD) which possess several parameters, corresponding to the various hadron coupling constants. In principle, if uniquely determined,

such parameters can be computed from QCD. Thus, it is useful to find ways to constrain the phenomenological QHD proceedure [2]. In this talk, we present the crossing and duality constraints in the analyses of kaon production and capture processes [3]. The procedure that we discuss here is quite general and readily applies to other hadron reactions. We concentrate on kaon induced reactions because precise experimental data on these processes will be obtained at CEBAF in the near future. Kaon photoproduction experiments are scheduled to be performed in the CEBAF Hall B endstation, whereas kaon electroproduction will be investigated in Halls A and C. All three Halls are projected to be completed in the next three years. Further, the study of kaon production and absorption should be valuable in constructing models for the kaon condensation in neutron stars. The topic of the kaon condensation is discussed by other speakers in this symposium [4]. Here, however, we simply emphasize that QHD models are, in general, very effective for analyzing nuclear astrophysics.

This talk will be presented in the following order. In the section II, we introduce the crossing relations in a simple model of Kp elastic scattering. In section III, the application to kaon photoproduction and radiative capture is presented. The isospin and parity symmetries of kaon photoproduction is discussed in section IV. In section V, the extension to kaon electroproduction is presented followed by our conclusions which are discussed in section VI.

II Crossing Relations in a Simple Model of Kp Elastic Scattering

Consider the K^-p elastic scattering as the s-channel process. Then, the Mandelstam variables [5] in this channel are given by

$$\begin{aligned} s_1 &= (q_1 + p_1)^2 \ , \\ t_1 &= (q_1' - q_1)^2 \ , \\ u_1 &= (p_1' - q_1)^2 \ , \end{aligned} \tag{II-1}$$

where q_1 (q_1') and p_1 (p_1') are the four momenta of the initial (final) K^--meson and proton, respectively. If the helicity of the initial (final) proton is labelled by λ (λ'), then the scattering amplitude is

$$\begin{aligned} &T^{(s)}_{\lambda\lambda'}(q_1, p_1, q_1', p_1') \ = \\ &\overline{u}(p_1', \lambda') \left[A^{(s)}(s_1, t_1, u_1) \ + \ \frac{\not{q}_1 + \not{q}_1'}{2} B^{(s)}(s_1, t_1, u_1)\right] u(p_1, \lambda) \ . \end{aligned} \tag{II-2}$$

By crossing the s-channel to the u-channel, we obtain the K^+p elastic scattering, which has the Mandelstam variables

$$\begin{aligned} s_2 &= (q_2 + p_2)^2 \ , \\ t_2 &= (q_2' - q_2)^2 \ , \\ u_2 &= (p_2' - q_2)^2 \ , \end{aligned} \tag{II-3}$$

where q_2 (q_2') and p_2 (p_2') are the four momenta of the initial (final) K^+-meson and proton, respectively. The initial (final) K^--meson in the s-channel is crossed to the final (initial) K^+-meson in the u-channel. The scattering amplitude in this

channel is then given by

$$T^{(u)}_{\lambda\lambda'}(q_2,p_2,q_2',p_2') \; = \qquad \text{(II-4)}$$
$$\overline{u}(p_2',\lambda')\,[A^{(u)}(s_2,t_2,u_2) \; + \; \frac{\not q_2 + \not q_2'}{2} B^{(u)}(s_2,t_2,u_2)]\; u(p_2,\lambda) \; .$$

The main idea of crossing is that the scattering amplitude is a universal, analytic function of the Mandelstam variables, hence there is only one amplitude for all channels. Thus, the scattering amplitudes in the s-channel and u-channel given by Eqs. (II-2) and (II-4) respectively are actually the same

$$T^{(s)}_{\lambda\lambda'}(q_1,p_1,q_1',p_1') \; = \; T^{(u)}_{\lambda\lambda'}(q_2,p_2,q_2',p_2') \; . \qquad \text{(II-5)}$$

Because the four-momenta in the s-channel and u-channel are related by $q_2 = -q_1'$, $p_2 = p_1$, $q_2' = -q_1$ and $p_2' = p_1'$, we now obtain the crossing relation given by [2]

$$T^{(u)}_{\lambda\lambda'}(q_2,p_2,q_2',p_2') \; = \; T^{(s)}_{\lambda\lambda'}(-q_2',p_2,-q_2,p_2') \; . \qquad \text{(II-6)}$$

While the physical kinematic region of one channel may correspond to the unphysical region of the other channel, the scattering amplitude governing the crossing related channels is universal. From Eqs. (II-2), (II-4) and (II-6), we obtain

$$\begin{aligned} A^{(u)}(s_2,t_2,u_2) &= A^{(s)}(u_2,t_2,s_2) \; , \qquad \text{(II-7)} \\ B^{(u)}(s_2,t_2,u_2) &= -B^{(s)}(u_2,t_2,s_2) \; . \end{aligned}$$

Likewise, the t-channel corresponds to the K^+K^- production in $p\overline{p}$ annihilation ($p\overline{p} \to K^+K^-$) and the amplitudes in the t-channel are related to those in the s-channel by crossing;

$$\begin{aligned} A^{(t)}(s_3,t_3,u_3) &= A^{(s)}(t_3,s_3,u_3) \; , \qquad \text{(II-8)} \\ B^{(t)}(s_3,t_3,u_3) &= -B^{(s)}(t_3,s_3,u_3) \; , \end{aligned}$$

where

$$\begin{aligned} s_3 &= (q_3+p_3)^2 \; , \\ t_3 &= (q_3'-q_3)^2 \; , \qquad \text{(II-9)} \\ u_3 &= (p_3'-q_3)^2 \; , \end{aligned}$$

and q_3, p_3, q_3' and p_3' are the four-momenta of the $\overline{p}$, p, K^+ and K^-, respectively.

To appreciate the utility of the crossing relations given by Eqs. (II-7) and (II-8), let's introduce a simple model [2] to describe the above three reactions, $K^-p \to K^-p$, $K^+p \to K^+p$ and $p\overline{p} \to K^+K^-$. The interaction Lagrangian density in this model is given by

$$\begin{aligned} \mathcal{L}_I \; = \; & ig_\Lambda\,[\,\overline{N}\gamma_5\Lambda\,K \; + \; \overline{K}\,\overline{\Lambda}\gamma_5 N\,] \qquad \text{(II-10)} \\ & + ig_\Sigma\,[\,\overline{N}\gamma_5\vec{\tau}\cdot\vec{\Sigma}\,K \; + \; \overline{K}\,\overline{\vec{\Sigma}}\cdot\vec{\tau}\gamma_5 N\,] \; , \end{aligned}$$

where

$$N = \begin{pmatrix} p \\ n \end{pmatrix} \; , \quad K = \begin{pmatrix} K^+ \\ K^0 \end{pmatrix} \; , \quad \vec{\Sigma} = \begin{pmatrix} \Sigma_1 \\ \Sigma_2 \\ \Sigma_3 \end{pmatrix} \; . \qquad \text{(II-11)}$$

Here, the Σ-baryons are given by

$$\begin{aligned} \Sigma^\pm &= \frac{\pm\Sigma_1 + i\Sigma_2}{\sqrt{2}} \; , \qquad \text{(II-12)} \\ \Sigma^0 &= \Sigma_3 \; , \end{aligned}$$

and the Λ-baryon is an isospin singlet. Using this model, one can obtain the s-channel amplitudes in the lowest order;

$$\begin{aligned} A^{(s)}(s_1,t_1,u_1) &= \sum_{Y=\Lambda,\Sigma} \frac{g_Y^2(M_Y - M_p)}{s_1 - M_Y^2} \; , \qquad \text{(II-13)} \\ B^{(s)}(s_1,t_1,u_1) &= -\sum_{Y=\Lambda,\Sigma} \frac{g_Y^2}{s_1 - M_Y^2} \; . \end{aligned}$$

Table I: Different sets of coupling constants. The first two columns are used in Sec. II for the purely hadronic calculations, while all four columns are used in Sec. III for the electromagnetic applications. Note that the Σ coupling constant, g_Σ, was determined from $G_\Sigma = \kappa_T g_\Sigma$ where G_Σ is given in Refs. 6 and 7 and $\kappa_T = -2.24$ is the dimensionless Σ-Λ transition moment factor.

Set	$\frac{g_\Lambda}{\sqrt{4\pi}}$	$\frac{g_\Sigma}{\sqrt{4\pi}}$	$\frac{G_V}{4\pi}$	$\frac{G_T}{4\pi}$
A (Ref. 6)	2.57	-0.679	0.105	0.064
B (Ref. 6)	2.49	-0.518	0.226	-0.062
C (Ref. 7)	2.04	0.554	0.247	-0.189

From the crossing relations given by Eqs. (II-7) and (II-8), one can also obtain the u-channel and t-channel amplitudes as follows;

$$A^{(u)}(s_2,t_2,u_2) = \sum_{Y=\Lambda,\Sigma} \frac{g_Y^2(M_Y - M_p)}{u_2 - M_Y^2} , \qquad \text{(II-14)}$$

$$B^{(u)}(s_2,t_2,u_2) = \sum_{Y=\Lambda,\Sigma} \frac{g_Y^2}{u_2 - M_Y^2} .$$

and

$$A^{(t)}(s_3,t_3,u_3) = \sum_{Y=\Lambda,\Sigma} \frac{g_Y^2(M_Y - M_p)}{t_3 - M_Y^2} , \qquad \text{(II-15)}$$

$$B^{(t)}(s_3,t_3,u_3) = \sum_{Y=\Lambda,\Sigma} \frac{g_Y^2}{t_3 - M_Y^2} .$$

The main point of this exercise is that crossing requires the same parameters, g_Λ and g_Σ, for all three different channels. This constraint plays an important role for obtaining the correct parameters in an effective field theory.

As an example, let's consider the three parameter sets listed in Table I. We have investigated the sensitivity of the K^-p elastic scattering cross section to

the uncertainty in the Λ and Σ coupling constants. In Fig. 1, we summarize our results by presenting three curves corresponding to three different coupling constant sets listed in Table I. These sets, labeled A, B and C were obtained from kaon photoproduction phenomenological analyses and will also be used in the next section that addresses crossing for electromagnetic hyperon processes. Only the first two columns are relevant to the hadronic calculations reported in this section. Because of the simplicity of our model, it is not surprising that none of the theoretical curves quantitatively describes the data [8] also shown in Fig. 1. The K^-p system, even at threshold, has several effects such as coupling to other open channels ($\Lambda\pi$ and $\Sigma\pi$) and excited hyperon states ($\Lambda^*$and Σ^*), especially the $\Lambda(1405)$ and $\Sigma(1520)$ which are known to be important. These have not been included because our thrust here is to document the utility of crossing in constraining dynamic model analyses. The key issue is that different channels (s,t or u) may reveal different and useful sensitivity to the same underlying model parameters. With this in mind, we now address the u-channel K^+p elastic and t-channel $p\bar{p} \to K^+K^-$ processes to determine their sensitivity to the same three sets of coupling constants.

Figure 2 summarizes our sensitivity study for K^+p elastic scattering. Again the same three sets of coupling constants are used. Notice that the sensitivity is somewhat different than that reflected by K^-p scattering in Fig.1. Figure 3 displays our sensitivity study for $p\bar{p} \to K^+K^-$ with the same three sets of coupling constants. Comparing Figs. 1, 2 and 3 further supports our claim that the sensitivity to model parameters is different for different channels.

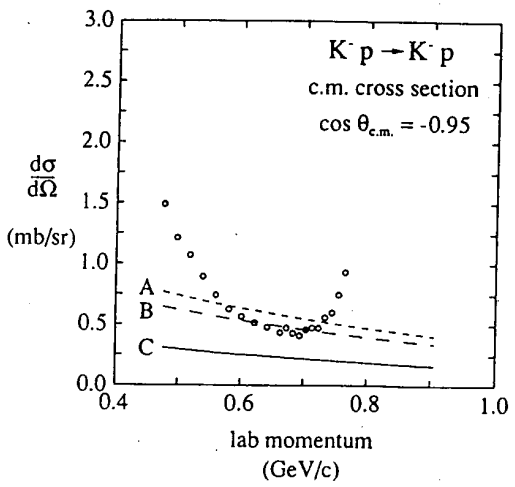

Figure 1: Theoretical and experimental (Ref. 8) (error bars are omitted) K^-p elastic scattering cross section. The different theoretical curves correspond to the three sets of coupling constants A (short dashed), B (long dashed), and C (solid) listed in Table I. Only the first two columns of Table I are used for the calculations displayed in Figs. 1-3.

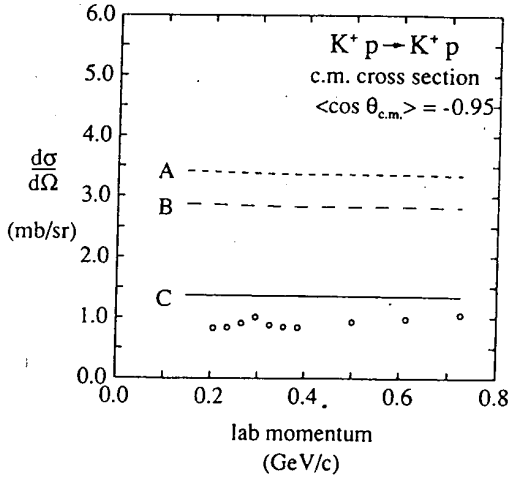

Figure 2: Same as Fig.1 for K^+p elastic scattering. Data from Ref. 9.

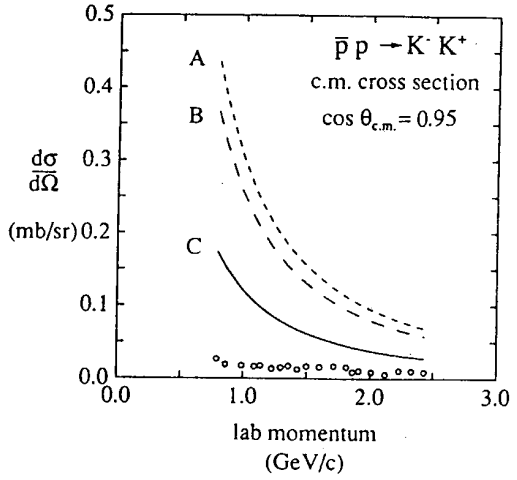

Figure 3: Same as Fig.1 for $p\bar{p} \to K^+K^-$. Data from Ref.10.

III Application to Kaon Photoproduction and Radiative Capture

We now apply our results to electromagnetic reactions and document the sensitivity of calculations for kaon photoproduction, $\gamma p \to K^+\Lambda$, to the full set of coupling constants listed in Table I. Because new, improved measurements are planned for these processes [at CEBAF, Japan's National Laboratory for High Energy Physics (KEK), and proposed North American "kaon factories"] and because these reactions entail electromagnetic coupling ($\alpha_e = e^2/4\pi \simeq \frac{1}{137}$), which is more amenable to our perturbative treatment, we have been motivated to include additional refinements.

As demonstrated in Refs. 6 and 11, a more realistic theoretical treatment can be obtained by extending the model to accommodate vector meson K^* exchange.

The purely hadronic interaction Lagrangian is now generalized to describe K^* exchange by adding

$$\mathcal{L}_I^{K^*} = \mathcal{L}_I^V + \mathcal{L}_I^T \ , \qquad \text{(III-1)}$$

where $\mathcal{L}_I^V$ and $\mathcal{L}_I^T$ are the vector and tensor interactions involving respective coupling constants $g_{K^*}^V$ and $g_{K^*}^T$:

$$\mathcal{L}_I^V = -ig_{K^*}^V \, (\bar{N}\gamma^\mu \Lambda \, K_\mu^* + \bar{K}_\mu^* \, \bar{\Lambda}\gamma^\mu N \,) \ , \qquad \text{(III-2)}$$

$$\mathcal{L}_I^T = \frac{-ig_{K^*}^T}{M_p + M_\Lambda}[\, \bar{N}\sigma^{\mu\nu}\Lambda(\nabla_\mu K_\nu^* - \nabla_\nu K_\mu^*) + (\nabla_\mu \bar{K}_\nu^* - \nabla_\nu \bar{K}_\mu^*)\bar{\Lambda}\sigma^{\mu\nu}N \,] \ . \qquad \text{(III-3)}$$

Here K_μ^* represents the vector kaon field which is an isospin doublet (we use the same isospin notation as for K defined previously), ∇_μ is the standard four-gradient and $\sigma^{\mu\nu}$ is defined by

$$\sigma^{\mu\nu} = \frac{i}{2}(\gamma^\mu\gamma^\nu - \gamma^\nu\gamma^\mu) \ . \qquad \text{(III-4)}$$

We now introduce the photon field A_μ with field strength tensor $F_{\mu\nu}$

$$F_{\mu\nu} = \nabla_\mu A_\nu - \nabla_\nu A_\mu \ . \qquad \text{(III-5)}$$

The presence of this field leads to the following electromagnetic interaction Lagrangian $\mathcal{L}_I^{em}$ which must be added to the Lagrangians specified by Eqs.(II-10) and (III-1):

$$\mathcal{L}_I^{em} = -e(J_p^\mu + J_K^\mu)A_\mu - (\mu_p \bar{p}\sigma^{\mu\nu}p + \mu_\Lambda \bar{\Lambda}\sigma^{\mu\nu}\Lambda + \mu_T \bar{\Lambda}\sigma^{\mu\nu}\Sigma^0)F_{\mu\nu} - \frac{g_{KK^*}^\gamma}{M}\epsilon^{\alpha\beta\gamma\delta}[\, K^+\nabla_\alpha K_\beta^{*+} + K^-\nabla_\alpha K_\beta^{*-} \,]\nabla_\gamma A_\delta \ , \qquad \text{(III-6)}$$

where M is a mass, arbitrarily taken to be 1 GeV, introduced to make the K^*-K electromagnetic coupling constant, $g_{KK^*}^\gamma$, dimensionless. The current J^μ and anomalous baryon (B) magnetic moments μ_B are given by

$$J_p^\mu = \bar{p}\gamma^\mu p \ \text{(proton current)} \ , \qquad \text{(III-7)}$$

$$J_K^\mu = i\,(K^-\nabla^\mu K^+ - K^+\nabla^\mu K^-) \ \text{(kaon current)} \ , \qquad \text{(III-8)}$$

$$\mu_p = \frac{e\kappa_p}{2M_p} \ \text{(proton moment)} \ , \qquad \text{(III-9)}$$

$$\mu_\Lambda = \frac{e\kappa_\Lambda}{2M_\Lambda} \ (\Lambda \text{ moment}) \ , \qquad \text{(III-10)}$$

$$\mu_T = \frac{e\kappa_T}{M_\Lambda + M_{\Sigma^0}} \ (\Sigma^0 \to \Lambda \text{ transition moment}) \ . \qquad \text{(III-11)}$$

From experiment, $\kappa_p = 1.79$, $\kappa_\Lambda = -0.73$, and $\kappa_T = -2.24$ (magnitude determined from the $5.8 \times 10^{-20} s$ lifetime for $\Sigma^0 \to \Lambda\gamma$; sign is inferred from the quark model).

We now apply these results beginning with K^+ photoproduction, $\gamma p \to K^+\Lambda$, which we take to be the s-channel. For clarity, in this section we denote the γ, p, K^+, and Λ four-momenta by q, p, k, and l, taking the γ, p, K^+, and Λ helicities by h, λ, and λ', respectively. Because the photon has unit spin, described by the polarization four-vector $\epsilon_\mu(q,h)$ the invariant transition matrix element $T_{h\lambda\lambda'}^{(s)}$ now contains four elementary amplitudes, A_i:

$$T_{h\lambda\lambda'}^{(s)}(q,p,k,l) = \bar{u}(l,\lambda')\,\gamma_5 \epsilon_\mu(q,h) N_i^\mu A_i^{(s)}\, u(p,\lambda) \ , \qquad \text{(III-12)}$$

with bilinear four-vectors N_i^μ given by

$$N_1^\mu = -\frac{1}{2}(\gamma^\mu \not{q} - \not{q}\gamma^\mu) \ , \qquad \text{(III-13)}$$

$$N_2^\mu = 2(p^\mu q\cdot l - l^\mu q\cdot p) \ , \qquad \text{(III-14)}$$

$$N_3^\mu = \gamma^\mu q\cdot p - p^\mu \not{q} \ , \qquad \text{(III-15)}$$

$$N_4^\mu = \gamma^\mu q\cdot l - l^\mu \not{q} \ . \qquad \text{(III-16)}$$

As reported in a previous study [11] we have calculated the elementary amplitudes by evaluating the S-matrix to second order for the above Lagrangian. These amplitudes, which are summarized in the Appendix, are functions of $s = (q+p)^2$, $t = (k-q)^2$, $u = (l-q)^2$, and the coupling constants which conveniently group into the effective parameters

$$G_\Sigma = \kappa_T \, g_\Sigma \ , \qquad \text{(III-17)}$$

$$G_V = g^\gamma_{KK^*} \, g^V_{K^*} \ , \qquad \text{(III-18)}$$

$$G_T = g^\gamma_{KK^*} \, g^T_{K^*} \ , \qquad \text{(III-19)}$$

which, along with g_Λ, have been phenomenologically analyzed previously [6, 7] and are listed in Table I. The spin-averaged c.m. cross section is

$$\frac{d\sigma^{(s)}}{d\Omega} = \frac{1}{4}\frac{M_p M_\Lambda}{(4\pi W)^2}\frac{|\mathbf{k}|}{|\mathbf{q}|}\sum_{h\lambda\lambda'} |T^{(s)}_{h\lambda\lambda'}|^2 \ , \qquad \text{(III-20)}$$

where $\mathbf{k}$, $\mathbf{q}$ are the kaon, photon c.m. momentum. Using trace techniques and computer algebra, Eq. (III-20) has been reduced and is specified in the Appendix of Ref. 2.

In Fig. 4 we display the photoproduction cross sections corresponding to the three sets of coupling constants in Table I. All curves provide a reasonable description of the data [12]. This is expected since each set was phenomenologically determined using this reaction. Again, our major thrust in this paper is not the physics of this reaction but to demonstrate that crossing can provide a powerful criterion for determining model completeness as parameters appropriately describing one channel may or may not provide a consistent description of crossed channels.

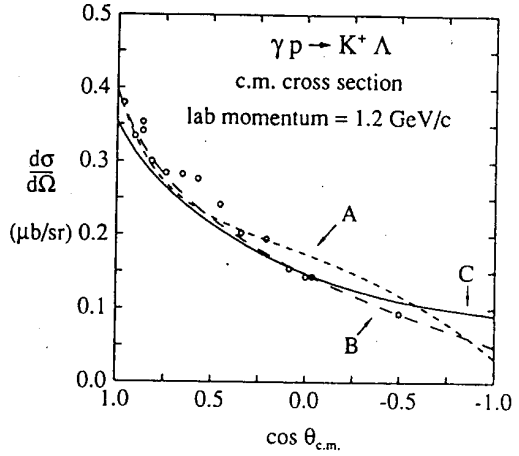

Figure 4: C.M. cross section for $\gamma p \to K^+\Lambda$ with the same labeling as Fig.1. All four columns of coupling constants in Table I are used for the calculations displayed in Figs. 4 and 5. Data from Ref. 12.

We now address the u-channel process $K^- p \to \gamma\Lambda$. Crossing the photon and kaon in the s-channel gives the, by now ubiquitous, relations for the physical u-channel having kaon momentum $\bar{k}$, photon momentum $\bar{q}$, photon helicity $\bar{h}$:

$$T^{(u)}_{\bar{h}\lambda\lambda'}(\bar{k},p,\bar{q},l) = T^{(s)}_{-\bar{h}\lambda\lambda'}(-\bar{q},p,-\bar{k},l) \ , \qquad \text{(III-21)}$$

$$T^{(u)}_{\bar{h}\lambda\lambda'}(\bar{k},p,\bar{q},l) = \bar{u}(l,\lambda')\,\gamma_5 \epsilon_\mu(\bar{q},\bar{h}) \times N^\mu_i A^{(u)}_i(s_2,t_2,u_2)\,u(p,\lambda) \ , \qquad \text{(III-22)}$$

where the N^μ_i are specified by Eqs. (III-13) - (III-16). Equating Eqs. (III-21) and (III-22) gives the crossing relations for the elementary amplitudes

$$A^{(u)}_i(s_2,t_2,u_2) = -A^{(s)}_i(u_2,t_2,s_2) \ , \quad i = 1,2,3,4 \ , \qquad \text{(III-23)}$$

with change of sign under $s_1 \to u_2$ and $u_1 \to s_2$ because the four-vectors N^μ_i also change for $q \to -\bar{q}$. We have confirmed these results through detailed di-

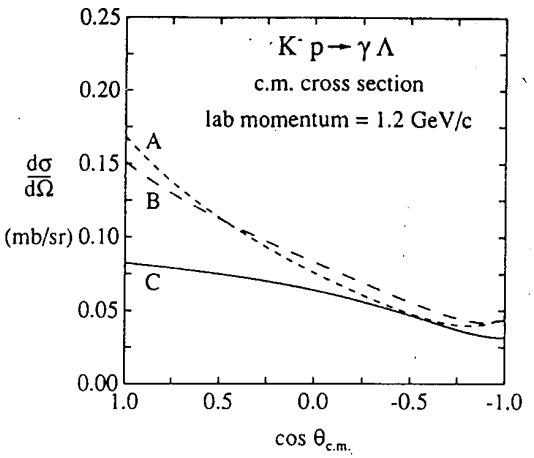

Figure 5: Same as Fig. 4, without data, for $K^-p \to \gamma\Lambda$.

agrammatic calculations. Accordingly, Eq. (III-23) completely determines the amplitudes. The spin-averaged c.m. cross section in the u-channel is

$$\frac{d\sigma^{(u)}}{d\Omega} = \frac{1}{2}\frac{M_p M_\Lambda}{(4\pi W)^2}\frac{|\bar{q}|}{|\bar{k}|}\sum_{\hbar\lambda\lambda'}|T^{(u)}_{\hbar\lambda\lambda'}|^2 , \qquad \text{(III-24)}$$

where W is the K^-p c.m. total energy and $\bar{k}$, $\bar{q}$ are the kaon, photon c.m. three-momenta, respectively. The spin-averaged transition probability is specified in the Appendix of Ref. 2.

In Fig. 5 we present our final sensitivity comparison. The significant result is that within the framework of a more sophisticated model, channel crossing again reveals informative differences among coupling constant sets which provide almost identical s-channel results. Unfortunately, there is very limited data for this reaction, as it would be interesting to see which phenomenological set, if any, would be favored. This represents a promising experiment for KEK and other proposed "kaon factories".

While cross section angular distributions are not available, the branching ratio for $K^-p \to \gamma\Lambda$ has been measured [13] to be within the range $(0.86 \pm 0.17) \times 10^{-3}$. We have calculated this ovservable for each coupling constant set and obtained the values: set A, 1.82×10^{-3}; set B, 1.68×10^{-3}; set C, 9.83×10^{-4}. Notice that again crossing reveals parameter sensitvity and that the value provided by set C is within the experimental limits. A more detailed theoretical treatment for this branching ratio has recently been published [14]. This work reports $K^-p \to \gamma\Lambda$ calculations for a K^-p atomic initial configuration and including additional diagrams corresponding to various N^* and Y^* exchanges. Although Ref. 14 computed branching ratios within the experimental range, their coupling constants were determined by kaon-induced hadronic processes which, as we have explicitly confirmed, do not reproduce kaon photoproduction data. This shortcoming, the inability to simultaneously describe both hadronic and electromagnetic processes involving kaons, has been noted earlier [15] and is most likely due to the model simplicity. As stated earlier in this paper, a perturbative, phenomenologica Lagrangian approach that explicitly includes only a few mesons and baryons is incomplete and for purely hadronic processes is probably incapable of providing a detailed description. Even for K^+p scattering, which is significantly constrained and simplified by strangeness conservation, there are several meson exchange contributions which, as examined in Ref. 16, are important and should be consistently included. Again, our thrust in this paper is not to advocate or critique a particular dynamic approach but rather to demonstrate the utility of crossing for the development of improved, realistic models, a topic we are currently investigating.

IV Isospin and Parity Symmetries in Kaon Photoproduction

In this section, we consider a few different hyperons in the kaon photoproduction processes, $\gamma p \to K^+ Y$ ($Y = \Lambda, \Sigma^0, \Lambda(1405)$). Because of the difference in the final state isospin and parity quantum numbers, one can make some interesting observations from the experimental data in conjunction with these symmetries.

IV.1 Isospin Symmetry

If we compare the two processes, $\gamma p \to K^+\Lambda$ and $\gamma p \to K^+\Sigma^0$, then we find an interesting difference in the final isospin states. For the isoscalar part of the photon, we have the following isospin assignment for the initial and final states.

	$\gamma\ p \to K^+\ \Lambda$		$\gamma\ p \to K^+\ \Sigma^0$	
I	$0\ \frac{1}{2}$	$\frac{1}{2}\ 0$	$0\ \frac{1}{2}$	$\frac{1}{2}\ 1$
I_{tot}	$\frac{1}{2}$	$\frac{1}{2}$	$\frac{1}{2}$	$\frac{1}{2}, \frac{3}{2}$

The main point here is that the kaon photoproduction process involves partly the electromagnetic interaction which can violate isospin conservation, and hence the total initial and final state isospins do not have to be the same. Thus, the isospin $\frac{3}{2}$ in the final $K^+\Sigma^0$ state in the above assignment is allowed and the Δ-excitation should be considered in this channel. For the isovector part of the photon, the isospin conservation of the strong interaction insures the Δ-excitation only in the $K^+\Sigma^0$ channel again. Thus, the principles of the isospin symmetry in the electromagnetic and strong interactions are essential to observe the Δ-excitation only in the Σ^0 production channel. In Figs. 6-8, the cross sections in various angles for the $\gamma p \to K^+\Sigma^0$ process are shown, demonstrating clear evidence of the spin 1/2 Δ-excitations.

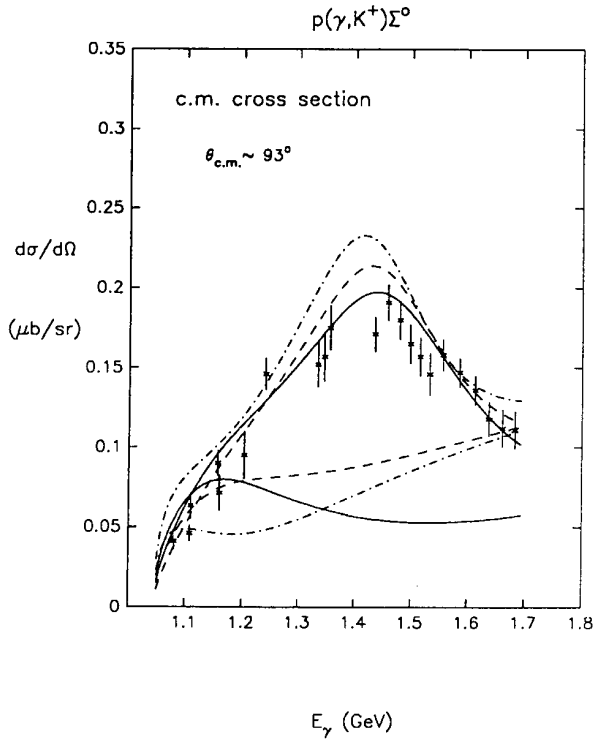

Figure 6: Energy dependence of the Σ^0 photoproduction cross section at $\theta_{c.m.} \sim 93°$. The solid, dashed and dashed-dotted lines represent crossing consistent models (a), (b) and (c) respectively, with parameters listed in Table II (see section V). The three lower curves were calculated neglecting the Δ resonances.

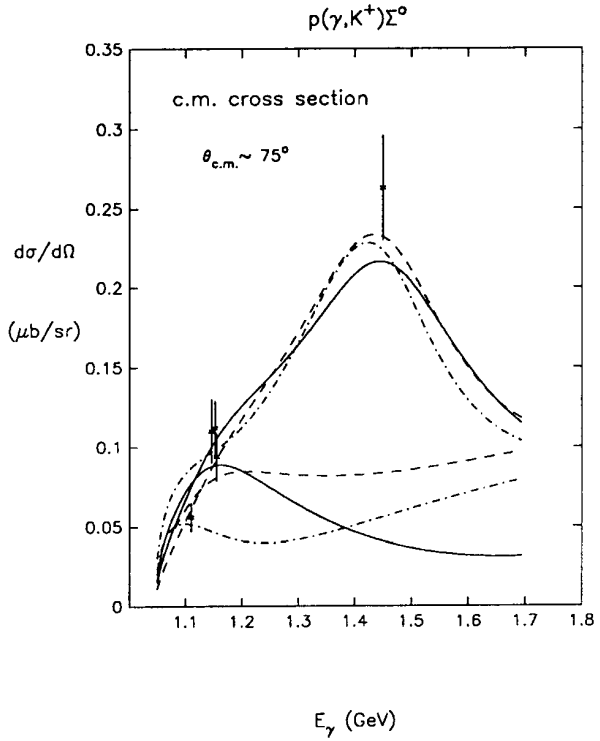

Figure 7: Energy dependence of the Σ^0 photoproduction cross section at $\theta_{c.m.} \sim 75^\circ$ with the same labeling as Fig.6.

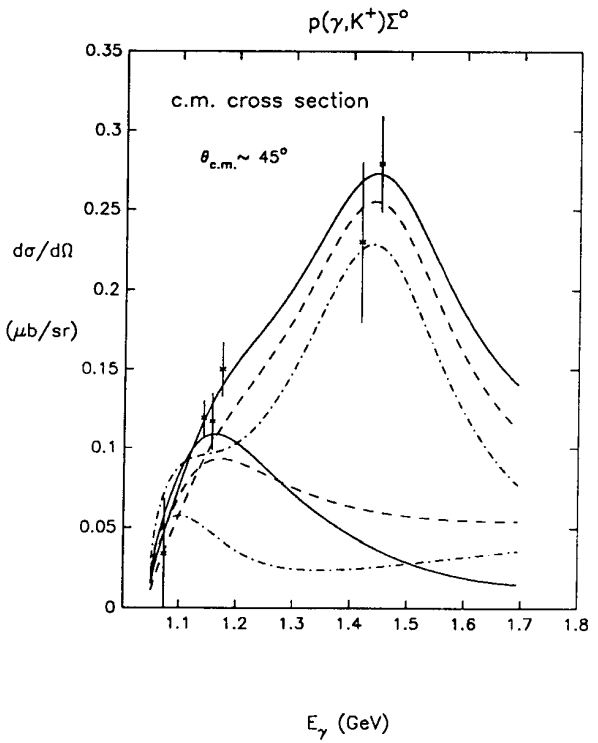

Figure 8: Energy dependence of the Σ^0 photoproduction cross section at $\theta_{c.m.} \sim 45^\circ$ with the same labeling as Fig.6.

IV.2 Parity

Now, let's compare the two processes, $\gamma p \to K^+\Lambda$ and $\gamma p \to K^+\Lambda(1405)$, which have opposite parity in the final state;

	$\gamma\ p \to K^+\ \Lambda$		$\gamma\ p \to K^+\ \Lambda(1405)$	
J^π	$1^-\ \frac{1}{2}^+$	$0^-\ \frac{1}{2}^+$	$1^-\ \frac{1}{2}^+$	$0^-\ \frac{1}{2}^-$
$\pi_{intrinsic}$	-1	-1	-1	$+1$

Since both the electromagnetic and strong interactions conserve parity, an amplitude decomposition in terms of eigenstates of angular momentum and parity reveals that partial waves are selected in the initial and final states to conserve total angular momentum and parity. For the dominant low energy E_0 multipole transition (i.e. even parity proton graph), we can easily conlude that the initial state should have predominantly P-wave contributions whereas the final states of $K^+\Lambda$ and $K^+\Lambda(1405)$ are P-wave and S-wave, respectively. Thus, we expect a relatively flat angular distribution in $K^+\Lambda(1405)$ production compared to $K^+\Lambda$ production. This is shown in Fig.9. Also, due to the S-wave dominance in $K^+\Lambda(1405)$ production, we expect [17] a small $\Lambda(1405)$ polarization (near threshold) compared to the polarization of Λ and Σ^0 production. The prediction is shown in Fig.10.

V Extension to Kaon Electroproduction

The considerations in the previous sections are now extended to kaon electroproduction [18] which is mediated by virtual photons. This means that the

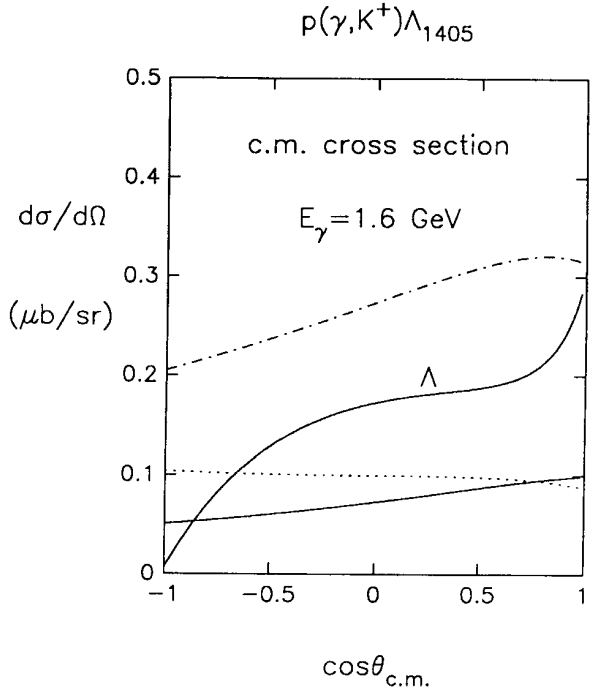

Figure 9: $\Lambda(1405)$ photoproduction cross section angular distribution at $E_\gamma = 1.6\ GeV$ showing the sensitivity to the unconstrained parameters of our model (solid line for $g_{KN\Lambda(1405)} = 1.5$; dashed-dotted line for $g_{KN\Lambda(1405)} = 3.0$). The dotted line demonstrates sensitivity to N^* resonances (with $g_{KN\Lambda(1405)} = 1.5$ and N^* coupling constants equal to zero).

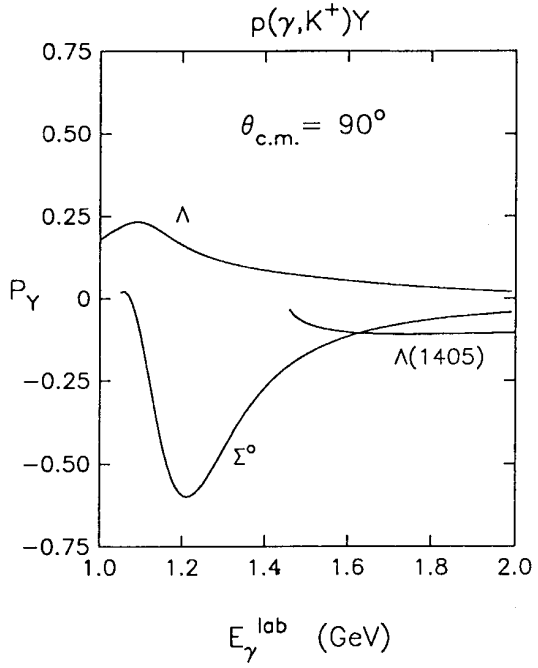

Figure 10: Energy dependence of the Λ, Σ^0 and $\Lambda(1405)$ polarizations at $\theta_{c.m.} = 90^\circ$ predicted by our model.

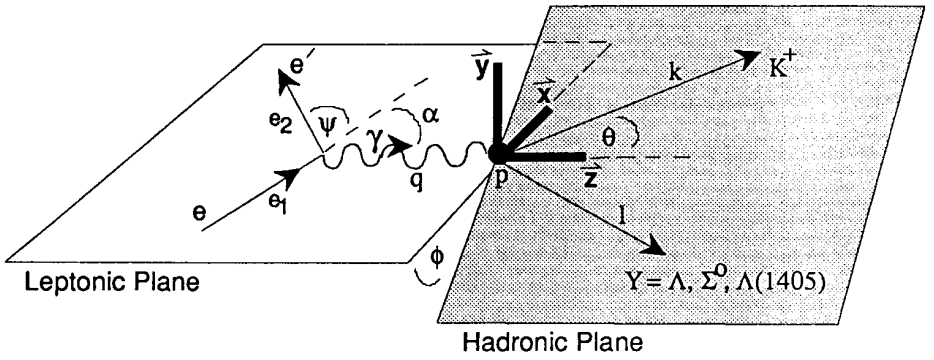

Figure 11: Laboratory frame kinematics for kaon electroproduction.

on-mass-shell condition of the photon, $q^2 = 0$, is now removed since q^2 is intrinsically negative ($q^2 < 0$) in the $ep \to e'K^+Y$ processes. Further, this permits longitudinal photon polarization degrees of freedom, increasing the number of independent bilinear four-vectors N_i^μ from 4 to 6. The two additional four-current operatiors, N_5^μ and N_6^μ, are

$$N_5^\mu = 2(p-l)^\nu(q^\mu q_\nu - q^2 g_\nu^\mu) \qquad \text{(V-1)}$$

$$N_6^\mu = \not{q} q^\mu - q^2 \gamma^\mu \ .$$

The electroproduction processes have been extensively studied [18, 19] using the laboratory frame kinematics shown in Fig.11. Because the entire leptonic current and attending phase space can be factorized, the electroproduction differential cross section can be related to the (virtual) photoproduction cross section $\frac{d\sigma_v}{d\Omega_K}$;

$$\frac{d^3\sigma}{d\Omega_{e'} dE_{e'} d\Omega_K} = \Phi_{e'} \frac{d\sigma_v}{d\Omega_K} \ , \qquad \text{(V-2)}$$

where

$$\Phi_{e'} = \frac{\alpha_e E_{e'} \left[(q\cdot p)^2 - q^2 M_p^2\right]^{1/2}}{2\pi^2 \left[(e_1\cdot p)^2 - M_e^2 M_p^2\right]^{1/2} q^2 \, (\epsilon - 1)} \ , \qquad \text{(V-3)}$$

and the transverse polarization parameter ϵ is given by

$$\epsilon = \frac{1}{1 - \frac{2q^2}{q^2} \tan^2 \frac{\psi}{2}} \ . \qquad \text{(V-4)}$$

A useful expression for the virtual photoproduction cross section involves a decompostion into factors where the ϕ dependence is explicit:

$$\frac{d\sigma_v}{d\Omega_K} = \frac{d\sigma_U}{d\Omega_K} + \epsilon \frac{d\sigma_P}{d\Omega_K} \sin^2\theta \cos 2\phi + \epsilon_L \frac{d\sigma_L}{d\Omega_K} + [2\epsilon_L(\epsilon+1)]^{1/2} \frac{d\sigma_I}{d\Omega_K} \sin\theta \cos\phi \ , \qquad \text{(V-5)}$$

where ϵ_L specifies the longitudinal polarization

$$\epsilon_L = -\frac{q^2}{q_0^2}\epsilon \ , \qquad \text{(V-6)}$$

and the U, P, L, I subscripts label the unpolarized, transversely polarized, longitudinally polarized and interference cross sections respectively. These cross sections are calculated by including the diagrams shown in Fig.12. The effective coupling constants for electromagnetic Λ, Σ^0 and $\Lambda(1405)$ hyperon production are summarized in Table II. Note that sets (a) and (c) include t-channel K^* resonances, while set (b) excludes them. As demonstrated in Figs.13-17, the K^* contributions are very important. Invoking duality [20], the K^* graphs are effectively equivalent to the excited baryon resonances in the s- and u-channel (neglected in our model), which are obviously important at higher (intermediate) energy. In particular these vector mesons carry additional angular momentum which in turn introduces more partial waves which are necessary at higher energies.

Another important point of extending the calculation to electroproduction processes is to provide crossing predictions for e^+e^- pair production in kaon capture reactions ($K^-p \to e^+e^-Y$). Since the threshold mass of the virtual photon to

Table II. Effective coupling constants for $Y = \Lambda$, Σ^0 and $\Lambda(1405)$ electromagnetic hyperon production.

		$Y=\Lambda$		$Y=\Sigma^0$			$Y=\Lambda(1405)$		
Diagram	*Effective Coupling*	(a)	(b)	(a)	(b)	(c)	(a)	(b)	(c)
p, K^+	g_{KNY}	8.427	4.127	-0.968	-0.329	-0.329	2.598	2.651	1.851
Λ	$\mu_{Y\Lambda}\, g_{KN\Lambda}$	-5.166	-2.530	13.592	6.657	6.657	1.161	-0.709	-1.241
Σ^0	$\mu_{Y\Sigma}\, g_{KN\Sigma}$	-1.561	-0.531	-0.784	-0.266	-0.266	0.813	0.281	$\pm$ 0.611
$\Lambda^*(1405)$	$\mu_{Y\Lambda^*}\, g_{KN\Lambda^*}$	0.358	-0.451	-2.181	-2.237	2.014	-1.143	-1.166	3.987
$N^*(1650)$	$\mu_{N^*p}\, g_{KN^*Y}$	0.213	0.453	-0.437	-0.426	0.514	28.062	15.489	-3.579
$N^*(1710)$	$\mu_{N^*p}\, g_{KN^*Y}$	0.323	0.875	-2.329	-2.143	1.235	-2.037	-1.915	0.423
$\Delta^*(1620)$	$\mu_{\Delta^*p}\, g_{K\Delta^*Y}$	-	-	0.161	0.161	-0.175	-	-	-
$\Delta^*(1900)$	$\mu_{\Delta^*p}\, g_{K\Delta^*Y}$	-	-	0.315	0.315	0.235	-	-	-
$\Delta^*(1910)$	$\mu_{\Delta^*p}\, g_{K\Delta^*Y}$	-	-	2.757	2.158	1.523	-	-	-
$K^*(892)$	$g_{K^*K}\, g^V_{K^*NY}$	2.032	0	-1.375	0	0	-0.399	0	-1.277
	$g_{K^*K}\, g^T_{K^*NY}$	-0.984	0	1.774	0	0	-0.218	0	0.251
$K_1(1270)$	$g_{K_1K}\, g^V_{K_1NY}$	-0.236	0	1.684	0	0	0.581	0	-0.517
	$g_{K_1K}\, g^T_{K_1NY}$	-2.175	0	-0.862	0	0	2.164	0	0.248

s- channel graphs:

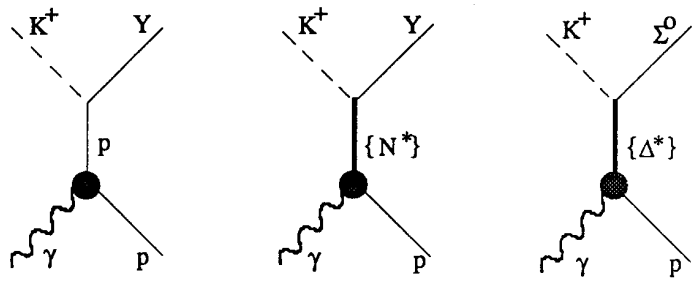

t- channel graphs:

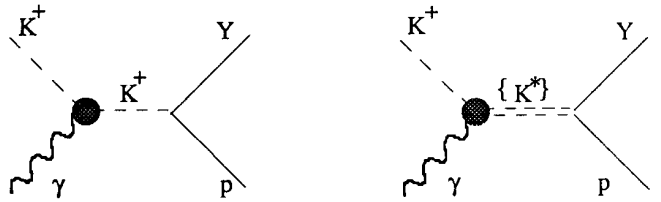

u- channel graphs:

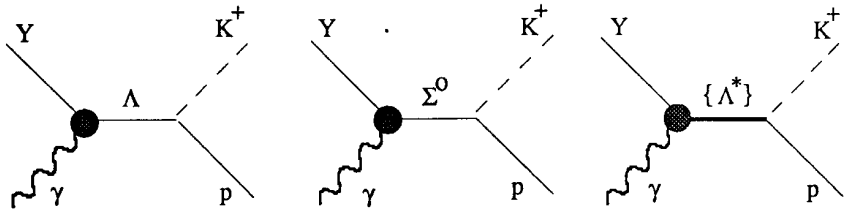

Figure 12: Diagrams used in our model for $p(\gamma, K^+)Y$ and $p(K^-, \gamma)Y$ for $Y = \Lambda, \Sigma^0, \Lambda(1405)$. $\{N^*\} \equiv \{N(1470), N(1650), N(1710)\}$, $\{\Lambda^*\} \equiv \{\Lambda(1405), \Lambda(1670), \Lambda(1800)\}$, $\{\Delta^*\} \equiv \{\Delta(1620), \Delta(1900), \Delta(1910)\}$, $\{K^*\} \equiv \{K^*(892), K_1(1270)\}$.

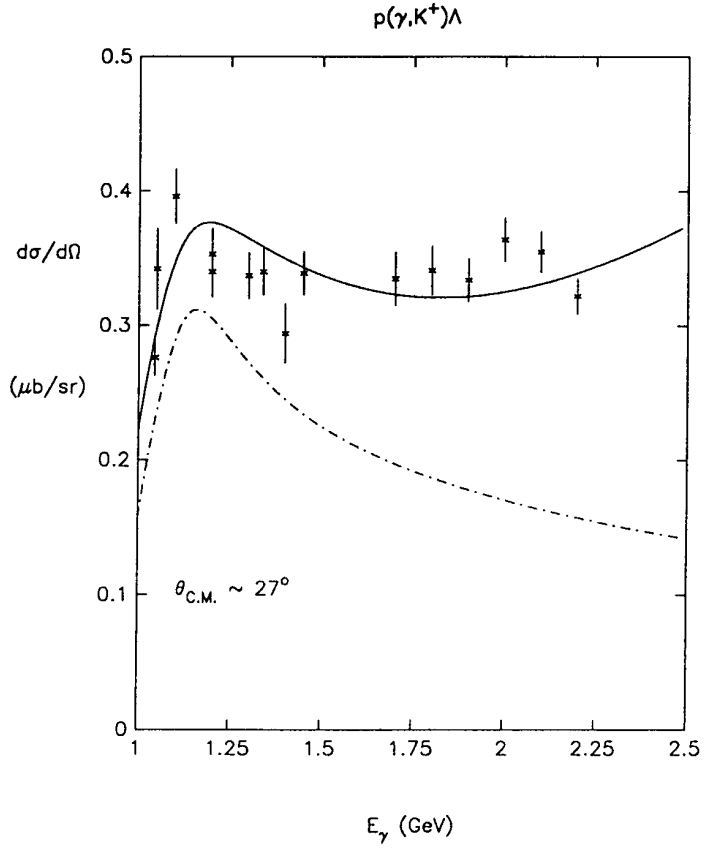

Figure 13: $p(\gamma, K^+)\Lambda$ photoproduction cross section at $\theta_{c.m.} \sim 27°$. The solid curve represents our new model, with the parameters specified in column (a) of Table II, whereas the dash-dotted curve represents our original 'naive' model, with the parameters in column (b) of Table II (which excludes the $K^*(892)$ and $K_1(1270)$ graphs).

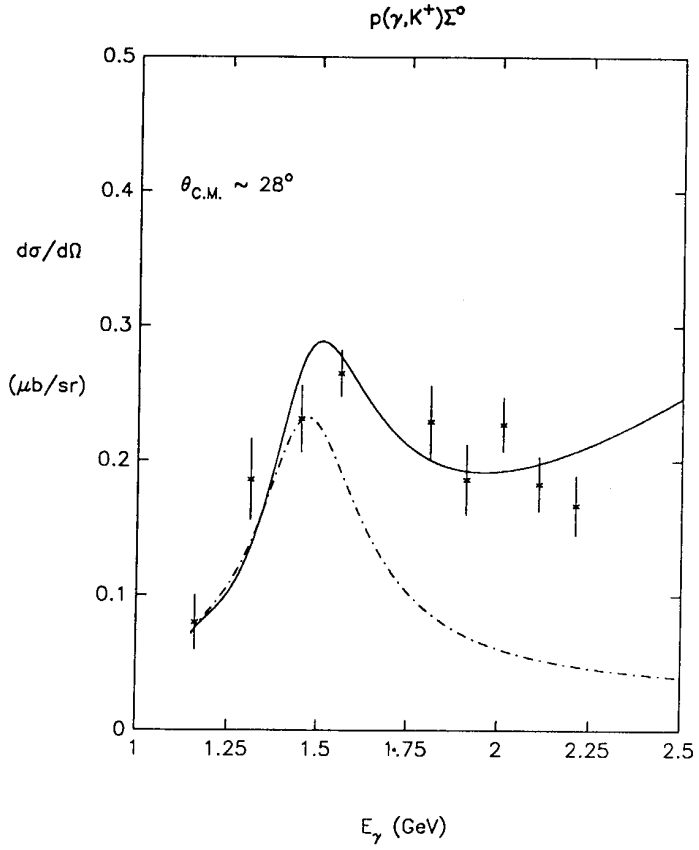

Figure 14: $p(\gamma, K^+)\Sigma^0$ photoproduction cross section at $\theta_{c.m.} \sim 28°$ with curves labeled (and hereafter unless otherwise specified) as in Fig. 13.

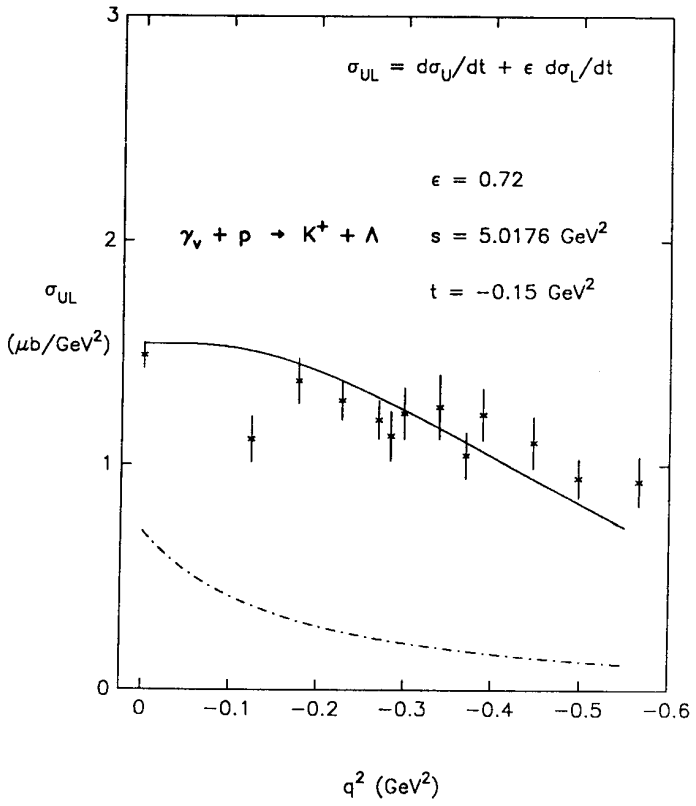

Figure 15: Unpolarized virtual photoproduction cross section (σ_{UL}) for Λ production as a function of q^2.

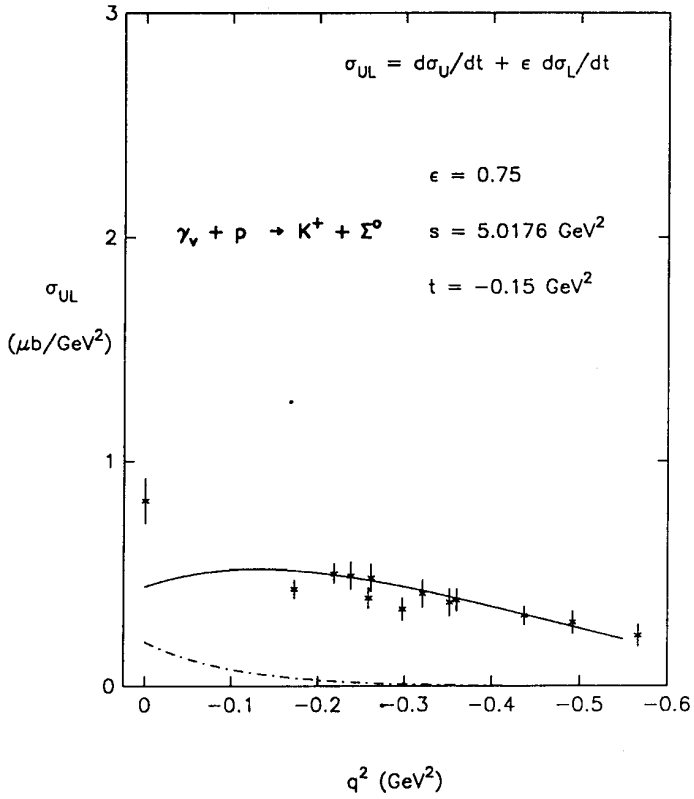

Figure 16: Unpolarized virtual photoproduction cross section (σ_{UL}) for Σ^0 production as a function of q^2.

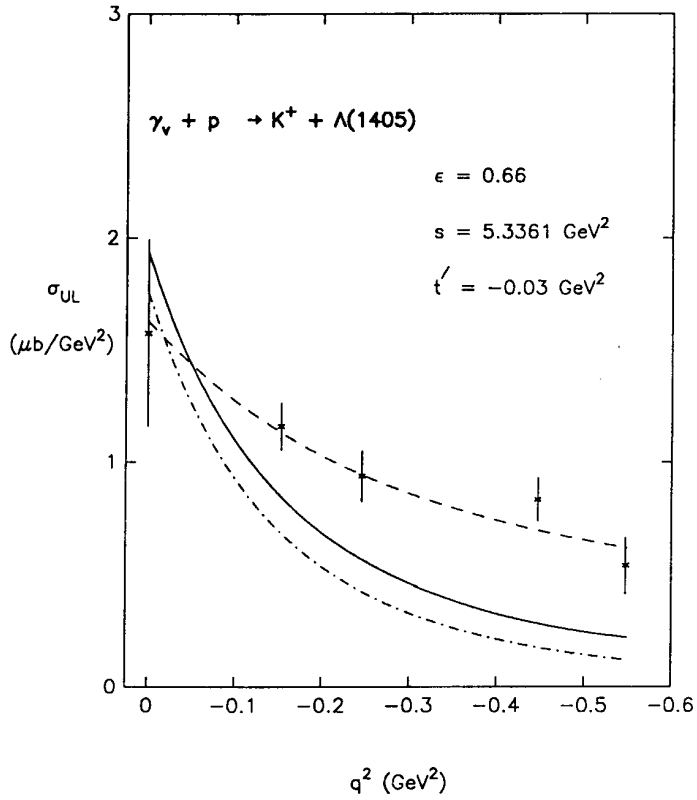

Figure 17: Unpolarized virtual photoproduction cross section (σ_{UL}) for $\Lambda(1405)$ production as a function of q^2. The solid, dashed-dotted and dashed lines corresponds to Table II sets (a), (b) and (c) respectively.

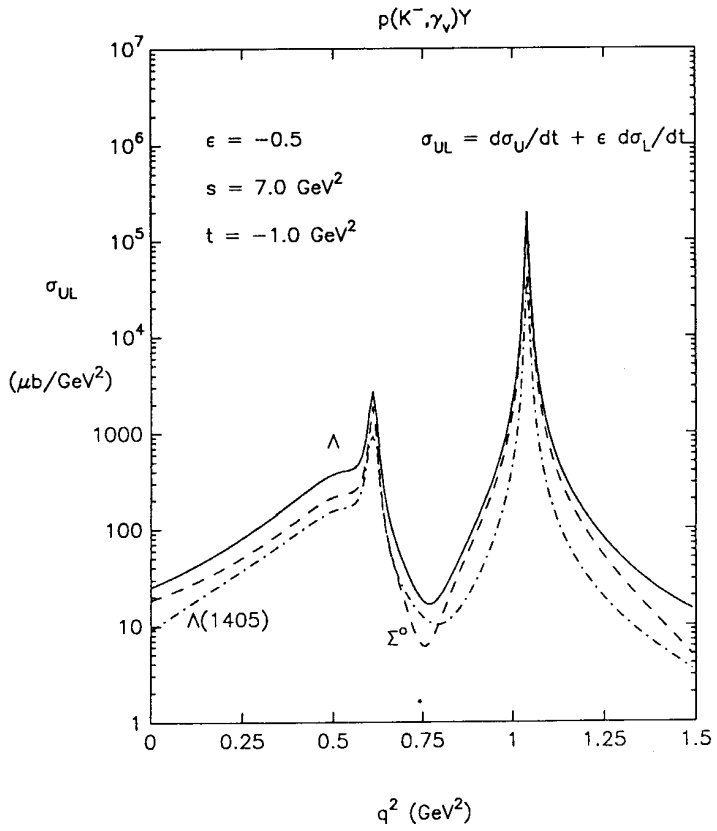

Figure 18: Two body virtual photon radiative capture cross section as a function of q^2 in the time-like region.

produce a e^+e^- pair in this process is only $4M_e^2$, i.e. $q^2 \geq 4M_e^2$, time-like form factors can be measured in the small q^2 region. The conventional measurement using hadron pair production in e^+e^- annihilation requires $q^2 \geq 4M_H^2$ making the very important low-q^2 time-like region inaccessible. Thus, meson capture processes are potentially very important for investigating time-like form factors in the (almost) entire $q^2 > 0$ region. Our recent predictions for the capture cross section using extended vector meson form factors are shown in Fig.18.

VI Conclusions

Even though QHD models have multiple parameters, the requirement of fundamental principles such as crossing can provide a stringent test of these parameters, which can lead to more sophisticate and realistic models. In this talk, we have shown that the symmetry considerations in weak, electromagnetic and strong interactions are also vital to build realistic models. As we discussed in the introduction, it is very important to construct such models to understand the history of the universe more accurately. The CEBAF laboratory is important for testing hadron models which can be used to describe the early universe at $10^{-5}s$. The connection of these hadron models to QCD is still missing, however, and linking the two is one of the most important future works.

Acknowledgments

This work was supported in part by the Korea Science and Engineering Foundation through Center for Theoretical physics, Seoul National University and in part by the Department of Energy, USA

References

[1] D.D. Clayton, Principles of Stellar Evolution and Nucleosynthesis, McGraw-Hill, New York, 1968.

[2] C.-R. Ji and S. R. Cotanch, Phys. Rev. C**38**, 2691 (1988).

[3] R. A. Williams, C.-R. Ji and S. R. Cotanch, Phys. Rev. D**41**, 1449 (1990); Phys. Rev. C**43**, 452 (1991); Phys. Rev. C**46**, 1617 (1992); Phys. Rev. C**48**, 1318 (1993).

[4] H. K. Lee's talk and D. P. Min's talk in this symposium.

[5] S. Mandelstam, Phys. Rev. **112**, 1344 (1958); **115**, 1741 (1959); **115**, 1752 (1959).

[6] H. Thom, Phys. Rev. **151**, 1322 (1966).

[7] R. A. Adelseck, C. Bennhold, and L. E. Wright, Phys. Rev. C**32**, 1681 (1985).

[8] M. Alston-Garnjost et al., Phys. Rev. D**21**, 1191 (1980).

[9] W. Cameron et al., Nucl. Phys. B**78**, 93 (1974).

[10] E. Eisenhandler et al., Nucl. Phys. B**96**, 109 (1975).

[11] S. S. Hsiao and S. R. Cotanch, Phys. Rev. C**28**, 1668 (1983).

[12] H. Genzel et al., Numerical Data and Functional Relationships in Science and Technology, Vol. 8 of Landolt-Bornstein (Springer-Verlag, Berlin, 1973).

[13] D. A. Whitehouse et al., Phys. Rev. Lett. **63**, 1352 (1989).

[14] R. L. Workman and H. Fearing, Phys. Rev. D**37**, 3117 (1988).

[15] J. Cohen, Phys. Lett. **153 B**, 367 (1985).

[16] J. Cohen, Phys. Lett. **192 B**, 291 (1987).

[17] S. R. Cotanch, R. A. Williams and C.-R. Ji, Colloque De Physique C6, 491 (1990).

[18] S. R. Cotanch, R. A. Williams and C.-R. Ji, Physica Scripta **49** (1992).

[19] R. A. Williams, PhD Thesis, NCSU (1993).

[20] F. M. Renard and Y. Renard, Nucl. Phys. B**25**, 490 (1971); V. De Alfaro, S. Fubini, G. Furlan and C. Rossetti, Currents in Hadron Physics, North-Holland Pub. Co. (1972), 571-662.